nature physics

Article

https://doi.org/10.1038/s41567-022-01910-7

Light emission from strongly driven many-body systems

Received: 21 December 2021

Accepted: 7 December 2022

Published online: 02 February 2023

Check for updates

Andrea Pizzi[1,2,6], Alexey Gorlach[3,6], Nicholas Rivera[1,4] ✉, Andreas Nunnenkamp[5] & Ido Kaminer[3] ✉

Strongly driven systems of emitters offer an attractive source of light over broad spectral ranges up to the X-ray region. A key limitation of these systems is that the light they emit is mostly classical. We overcome this constraint by building a quantum-optical theory of strongly driven many-body systems, showing that the presence of correlations among the emitters creates emission of non-classical many-photon states of light. We consider the example of high-harmonic generation, by which a strongly driven system emits photons at integer multiples of the drive frequency. In the conventional case of uncorrelated emitters, the harmonics are in an almost perfectly multi-mode coherent state lacking any correlation between harmonics. By contrast, a correlation of the emitters before the strong drive is converted into non-classical features of the output light, including doubly peaked photon statistics, ring-shaped Wigner functions and correlations between harmonics. We propose schemes for implementing these concepts, creating the correlations between emitters via an interaction between them or their joint interaction with the background electromagnetic field. Our work paves the way towards the engineering of novel states of light over a broadband spectrum and suggests high-harmonic generation as a tool for characterizing correlations in many-body systems with attosecond temporal resolution.

The creation and control of many-photon quantum states of light are important problems with applications across the natural sciences. Realizations of squeezed quantum light states open new avenues in spectroscopy and metrology, providing novel information on samples[1] and enabling highly sensitive measurements beyond classical noise limits (for example, in the detection of gravitational waves[2,3]). At the same time, encoding quantum information on the quantum state of light facilitates applications in quantum computing, simulation and communication[4]. Several pioneering investigations have demonstrated a range of many-photon quantum states of light such as squeezed light[2,3,5–7], bright squeezed vacuum[8–11], displaced Fock states[12], Schrödinger kitten[13,14] and cat states[15,16], subtracted squeezed states[17] and others[18]. Many of the established techniques for generating quantum light at optical frequencies rely on materials with a non-linear optical response. Such non-linear materials can be typically described using a 'perturbative' non-linear response, where the induced polarization is, for example, quadratic or cubic in the applied electric field.

At the other extreme of non-linear optics are 'non-perturbative' or 'strong-field' effects such as high-harmonic generation (HHG), in which a very intense optical pulse creates radiation at very high frequencies, even beyond hundred fold the frequency of the drive[19,20]. As such, HHG is an attractive source of ultra-short pulses of high-frequency light. The potential of HHG for the generation of non-classical high-frequency light has, however, remained largely unexpressed. In fact, many

[1]Department of Physics, Harvard University, Cambridge, MA, USA. [2]Cavendish Laboratory, University of Cambridge, Cambridge, UK. [3]Solid State Institute and Faculty of Electrical and Computer Engineering, Technion–Israel Institute of Technology, Haifa, Israel. [4]Massachusetts Institute of Technology, Cambridge, MA, USA. [5]Faculty of Physics, University of Vienna, Vienna, Austria. [6]These authors contributed equally: Andrea Pizzi and Alexey Gorlach. ✉e-mail: nrivera@fas.harvard.edu; kaminer@technion.ac.il

https://doi.org/10.1038/s41567-022-01910-7

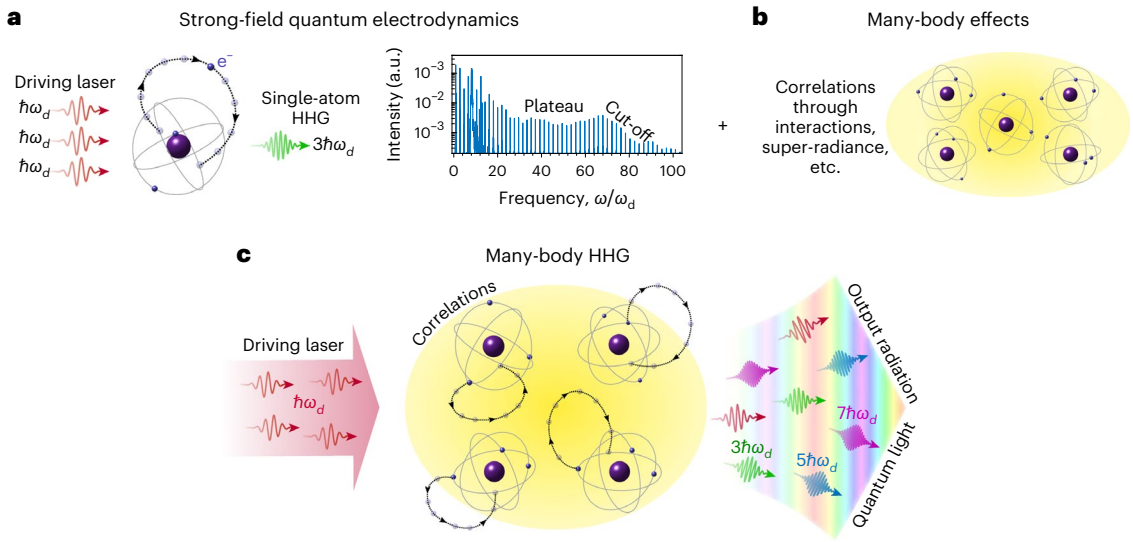

Fig. 1 | Quantum theory of light emission by strongly driven many-body atomic systems. a, HHG can be understood as a single-particle, strong-field three-step process: (1) an intense drive laser tears off an electron from the atom, (2) the electron is accelerated by the electric field and (3) the electron recombines with the atom, converting its energy into an energetic photon at higher harmonics. The spectrum features are peaks at the odd harmonics, a characteristic plateau and a cut-off. **b**, The many-body correlations among the atoms can arise from spontaneous collective emission (super-radiance) or inter-atomic interactions. **c**, Our theory marries the description of many-body effects with that of strong-field physics, giving access to unique quantum properties of the emitted light.

past semi-classical approaches[21–23] and more recent fully quantized ones[14,24–26] have established that the output harmonics in HHG are in an almost precisely coherent (thus, classical) state (apart from the notable exception of post-selected cat states in the driving frequency[14]). Nonetheless, these works all focus on the scenario of uncorrelated emitters, leaving open important questions about many-body aspects underlying HHG, in particular the extent to which correlations between the emitters affect the state of light created in the HHG process.

In this work, we develop a quantum-optical theory of light emission by strongly driven many-body systems. We use this theory to show that many-body correlations in the emitters can render the output radiation strongly non-classical (Fig. 1). To demonstrate this concept, we show that HHG from a correlated many-body state of emitters features exotic photonic states, for instance, super-Poissonian and doubly peaked photon number statistics, ring-shaped Wigner functions and strong correlations between harmonics. These features strongly contrast with conventional HHG from uncorrelated emitters, in which the output harmonics are described by almost perfectly Poissonian photon statistics, Gaussian Wigner functions and uncorrelated harmonics.

Indeed, the quantum state of the emitted light can be shaped by creating different correlations among the emitters. We show this general idea by investigating two concrete scenarios, one in which correlations among the emitters are induced through collective super-radiant emission and one in which they arise from dipole–dipole-type interactions. Our study makes the first step towards the creation of bright high-frequency light with engineered quantum properties. Applying this concept in reverse, characterizing the quantum photonic state of the emitted light will enable to infer the many-body correlations of the material with high temporal resolution.

Results

We develop a quantum-optical theory that describes the interaction among an intense driving field, a quantum-correlated (many-body) atomic system and the quantized radiation emitted from it. For a given initial atomic condition, our theory produces a full portrait of the emitted quantum light, including the Wigner function, photon number statistics and correlation between different harmonics. First, we consider the standard scenario in which the atoms are initially in their ground state and show that the emission resulting from the strong drive is in this case essentially coherent: the Wigner function and photon statistics of the harmonics are almost Gaussian and Poissonian, respectively, and the different harmonics are uncorrelated. Second, we investigate the effect of strong atomic correlations on the output radiation, showing that, when the emitters are initially in a correlated (and thus non-separable) many-body state, the output radiation becomes non-classical, featuring non-Gaussian Wigner functions, non-Poissonian photon statistics and correlated harmonic pairs. Third, we propose two experimentally relevant schemes exploiting inter-atomic interactions and super-radiance, respectively, to induce correlations in the atomic initial condition, resulting in controllably non-classical output radiation. An expanded and detailed version of the following theory is presented in Supplementary Sects. S1–S6. In the following, Hartree atomic units ($m_e = \hbar = e = a_0 = 1$ and $c = 137$) are used unless otherwise specified.

Quantum theory of strongly driven many-body systems

We consider N microscopic emitters (henceforth referred to as 'atoms' for convenience) interacting with a strong driving field. The Hamiltonian describing the system reads

$$\hat{H} = \sum_{i=1}^{N} \hat{H}^i_{\mathrm{atom}} + \sum_{i=1}^{N} \hat{\mathbf{d}}_i \cdot \hat{\mathbf{E}}(\mathbf{r}_i) + \hat{H}_{\mathrm{F}}, \tag{1}$$

where $\mathbf{r}_i$ and $\hat{\mathbf{d}}_i$ are the position and dipole moment of the ith atom, respectively, $\hat{H}_{\mathrm{F}} = \sum_{\mathbf{k}\sigma} \hbar\omega_{\mathbf{k}} \hat{a}^\dagger_{\mathbf{k}\sigma} \hat{a}_{\mathbf{k}\sigma}$ is the free-field Hamiltonian, with $\hat{a}^\dagger_{\mathbf{k}\sigma}$ and $\hat{a}_{\mathbf{k}\sigma}$ the creation and annihilation operators of a photon with wavevector $\mathbf{k}$ and polarization σ, respectively, and $\hat{H}^i_{\mathrm{atom}}$ is the single-particle Hamiltonian describing the outermost electron of the ith atom. The eigenvalue problem $\hat{H}^i_{\mathrm{atom}} |m\rangle = w_m |m\rangle$ is solved via standard space discretization procedures, resulting in a discrete single-particle spectrum composed of hundreds of levels, most of which are in the continuum, $w_m > 0$ (Supplementary Sect. S1).

The atomic system is driven with a laser whose field we take as a multi-mode coherent state $|\psi_{\mathrm{laser}}(t)\rangle = \prod_{\mathbf{k}} |\alpha_{\mathbf{k}} e^{i\omega_{\mathbf{k}} t}\rangle$, where $\alpha_{\mathbf{k}}$ is

the parameter of a coherent state with frequency $\omega_{\mathbf{k}}$. Using a unitary transformation (generated by a displacement operator)[26–30], the electric field $\hat{\mathbf{E}}(\mathbf{r},t)$ can be separated into a classical part $\mathbf{E}_{\mathrm{c}}(\mathbf{r},t)=\langle\psi_{\mathrm{laser}}(t)|\hat{\mathbf{E}}(\mathbf{r})|\psi_{\mathrm{laser}}(t)\rangle$ and a quantum part $\hat{\mathbf{E}}_{\mathrm{q}}(\mathbf{r},t)=-\sum_{\mathbf{k}\sigma}\boldsymbol{\varepsilon}_{\mathbf{k}\sigma}\left(g_{\mathbf{k}\sigma}e^{\mathrm{i}\mathbf{k}\cdot\mathbf{r}}\hat{a}_{\mathbf{k}\sigma}(t)+g^{*}_{\mathbf{k}\sigma}e^{-\mathrm{i}\mathbf{k}\cdot\mathbf{r}}\hat{a}^{\dagger}_{\mathbf{k}\sigma}(t)\right)$, where $g_{\mathbf{k}\sigma}=\mathrm{i}\sqrt{\frac{2\pi\omega_{\mathbf{k}}}{V}}$, $\boldsymbol{\varepsilon}_{\mathbf{k}\sigma}$ is the polarization vector of the mode $\mathbf{k}\sigma$, and V is the volume. The term $\hat{\mathbf{E}}_{\mathrm{q}}$ represents quantum fluctuations of the electric field. We are interested in describing emission in vacuum, for which $V\to\infty$ and the modes are continuous. Under the action of the displacement operator, the initial photonic state changes from $|\psi_{\mathrm{laser}}\rangle$ to the vacuum with zero photons $|0\rangle$, and the photonic state only describes the radiation on top of the drive laser. Assuming the dipoles $\hat{\mathbf{d}}_i$ to be polarized in the x direction, the light–matter coupling term in equation (1) can be rewritten as $\sum_i^N\hat{x}_i\hat{E}(\mathbf{r}_i)$, where $\hat{E}=\hat{\mathbf{E}}\cdot\mathbf{e}_x$. In its single-particle version with $N=1$ atom, the above model is known to capture the main features of HHG, including the characteristic plateau and cut-off of the emission spectrum[21,22] (Fig. 1b). Here, we wish to investigate the effects that many-body atomic correlations for $N\gg1$ have on the emitted output light. Due to the exponential (in N) size of the Hilbert space, such a many-body problem is in general a formidable one. We make it tractable by considering the simplest yet far from trivial scenario, one in which the spatial arrangement of the atoms is negligible. In this case, the state of the system can remain symmetric, meaning invariant under any permutation of the atoms, thus making the atoms effectively indistinguishable. While the assumption of indistinguishable atoms is physically justified in some cases, for example, when the atoms are in a small volume with respect to the involved interaction ranges and wavelengths, it can qualitatively describe multiple many-body phenomena even when not fully justified, similarly to what happens for instance for super-radiance[31,32], spin squeezing[33] and countless equilibrium phase transitions[34,35]. Indeed, this assumption opens the way to much analytical progress, which brings the ultimate numerical simulation of the system into reach and greatly facilitates physical intuition on the core involved physics.

The first key step is to note that, thanks to the atoms' permutational symmetry above, and according to a procedure analogous to second quantization, the state of the atomic system can be expressed in terms of atomic Fock states $|\mathbf{n}\rangle=|n_1,n_2,\ldots,n_m,\ldots\rangle$ with n_m the number of atoms in the mth single-particle level of $\hat{H}^{i}_{\mathrm{atom}}$ (Supplementary Sect. S2). In terms of standard bosonic creation and annihilation operators $\hat{b}^{\dagger}_m$ and $\hat{b}_m$, these states read $|\mathbf{n}\rangle=\left(\prod_m\left(\hat{b}^{\dagger}_m\right)^{n_m}/\sqrt{n_m!}\right)|0\rangle$, whereas the Hamiltonian in equation (1) yields

$$\hat{H}=\hat{\mathbf{b}}^{\dagger}W\hat{\mathbf{b}}-\left(E_{\mathrm{c}}+\hat{E}_{\mathrm{q}}\right)\hat{\mathbf{b}}^{\dagger}D\hat{\mathbf{b}}+\sum_{\mathbf{k}\sigma}\omega_{\mathbf{k}}\hat{a}^{\dagger}_{\mathbf{k}\sigma}\hat{a}_{\mathbf{k}\sigma}, \tag{2}$$

where W is a diagonal matrix with single-atom energies as entries, namely $W_{mn}=\delta_{mn}w_m$, D is a dipole matrix with entries $D_{mn}=\langle m|\hat{x}|n\rangle$ and where we called $\hat{\mathbf{b}}=\left(\hat{b}_1;\ \hat{b}_2;\ \ldots\right)$ the column vector of bosonic annihilation operators and $\hat{\mathbf{b}}^{\dagger}=\left(\hat{b}^{\dagger}_1,\hat{b}^{\dagger}_2,\ldots\right)$ the row vector of bosonic creation operators. In particular, the first two modes, $\hat{b}_1$ and $\hat{b}_2$, refer to the single-particle ground and first excited states $|g\rangle$ and $|e\rangle$, respectively. The Heisenberg equations associated with equation (2) read

$$\begin{cases}\frac{\mathrm{d}\hat{\mathbf{b}}}{\mathrm{d}t}=-\mathrm{i}\left(W-\left(E_{\mathrm{c}}+\hat{E}_{\mathrm{q}}\right)D\right)\hat{\mathbf{b}},\\ \frac{\mathrm{d}\hat{a}_{\mathbf{k}\sigma}}{\mathrm{d}t}=-\mathrm{i}\omega_{\mathbf{k}}\hat{a}_{\mathbf{k}\sigma}+\mathrm{i}g^{*}_{\mathbf{k}\sigma}\boldsymbol{\varepsilon}_{\mathbf{k}\sigma}\hat{\mathbf{b}}^{\dagger}D\hat{\mathbf{b}}.\end{cases} \tag{3}$$

To solve equation (3) we neglect the quantized part of the field $\hat{E}_{\mathrm{q}}$ in favour of the strong classical drive E_{c}, as is customary for HHG[22,36–38]. Indeed, this makes the atomic equation linear, which allows us to write

$$\hat{\mathbf{b}}(t)=F(t)\,\hat{\mathbf{b}}(0),\qquad F(t)=T\exp\left(-\mathrm{i}\int_0^t\left(W-E_{\mathrm{c}}(\tau)D\right)\mathrm{d}\tau\right), \tag{4}$$

a time evolution matrix, and T denoting time ordering. As for the photons, integrating the second equation in equation (3), and plugging equation (4) in, we get

$$\hat{a}_{\mathbf{k}\sigma}(t)=\hat{a}_{\mathbf{k}\sigma}(0)+\mathrm{i}g^{*}_{\mathbf{k}\sigma}\boldsymbol{\varepsilon}_{\mathbf{k}\sigma}\hat{\mathbf{b}}^{\dagger}(0)\,\tilde{D}(\omega_{\mathbf{k}})\,\hat{\mathbf{b}}(0). \tag{5}$$

where $\tilde{D}(\omega)=\int_0^t\mathrm{d}\tau\mathrm{e}^{\mathrm{i}\omega(\tau-t)}F^{\dagger}(\tau)DF(\tau)$. Considering only initial conditions with atoms in the two lowest single-particle states $|g\rangle$ and $|e\rangle$, we can effectively make the replacements $\hat{\mathbf{b}}^{\dagger}(0)\to\left(\hat{b}^{\dagger}_1(0),\hat{b}^{\dagger}_2(0)\right)$, $\hat{\mathbf{b}}(0)\to\begin{pmatrix}\hat{b}_1(0)\\ \hat{b}_2(0)\end{pmatrix}$ and $\tilde{D}\to\tilde{d}=\begin{pmatrix}\tilde{d}_{11}&\tilde{d}_{12}\\ \tilde{d}_{21}&\tilde{d}_{22}\end{pmatrix}$, which will henceforth be implicit in our notation. That is, for this class of initial conditions, the information contained in the $M\times M$-dimensional matrix F, which accounts for all the atomic levels including the continuum, gets compressed into the 2×2-dimensional matrix $\tilde{d}$. Next, we introduce the mode $\hat{a}_n$ of the nth harmonic as a normalized sum $\hat{a}_n=\frac{1}{\sqrt{\mathcal{N}}}\sum_{\mathbf{k}\in n}\hat{a}_{\mathbf{k}\sigma}(t_{\mathrm{f}})$, with t_{f} the time at which the pulse is over, and running over wavevectors $\mathbf{k}$ within a given solid angle $\mathrm{d}\Omega$ and with frequency $\omega_{\mathbf{k}}$ within the range $\left(n\omega_{\mathrm{d}}-\frac{\mathrm{d}\omega}{2},\ n\omega_{\mathrm{d}}+\frac{\mathrm{d}\omega}{2}\right)$, which should be thought of as those characterizing a detector used to collect the output light. Enforcing $\left[\hat{a}_n,\ \hat{a}^{\dagger}_n\right]=1$, we find $\mathcal{N}=\frac{n^2\omega_{\mathrm{d}}^2V\mathrm{d}\Omega}{(2\pi)^3c^3}\mathrm{d}\omega$ and get

$$\hat{a}_n=\hat{a}_n(0)+\hat{\mathbf{b}}^{\dagger}(0)\,d_n\hat{\mathbf{b}}(0), \tag{6}$$

with $d_n=\sqrt{\frac{\mathrm{d}\Omega}{4\pi}\frac{n^3\omega_{\mathrm{d}}^3}{\pi c^3}\mathrm{d}\omega}\,\tilde{d}(n\omega_{\mathrm{d}})$. We can decompose the matrix d_n in terms of Pauli matrices as $d_n=\alpha_n+(\mathbf{u}_n+\mathrm{i}\mathbf{v}_n)\cdot\boldsymbol{\sigma}$, where $\alpha_n=\frac{N}{2}\mathrm{Trace}(d_n)$ is a complex number, $\mathbf{u}_n$ and $\mathbf{v}_n$ are two three-component real vectors and $\boldsymbol{\sigma}=(\sigma_x,\ \sigma_y,\ \sigma_z)$ is the vector of Pauli matrices. We note that $N=\hat{\mathbf{b}}^{\dagger}(0)\,\hat{\mathbf{b}}(0)$ and that $\hat{\mathbf{S}}=\left(\hat{S}_x,\ \hat{S}_y,\ \hat{S}_z\right)=\sum_j^N\hat{\boldsymbol{\sigma}}_j=\hat{\mathbf{b}}^{\dagger}(0)\,\boldsymbol{\sigma}\hat{\mathbf{b}}(0)$, with $\hat{\boldsymbol{\sigma}}_j=\left(|e\rangle_j\langle g|_j+|g\rangle_j\langle e|_j,\ \mathrm{i}\left(|g\rangle_j\langle e|_j-|e\rangle_j\langle g|_j\right),\ |e\rangle_j\langle e|_j-|g\rangle_j\langle g|_j\right)$ the Pauli operators describing the transition between each atom's ground and first excited states $|g\rangle$ and $|e\rangle$, respectively. We can thus rewrite equation (6) in terms of standard collective spin operators for N spins 1/2 as

$$\hat{a}_n=\hat{a}_n(0)+\alpha_n+(\mathbf{u}_n+\mathrm{i}\mathbf{v}_n)\cdot\hat{\mathbf{S}}. \tag{7}$$

Equation (7) enables to present in a compact form some of the main achievements of our theory. This equation directly links the initial state of the atoms $\hat{\mathbf{S}}$ to the output state of the photons $\hat{a}_n$, which is thus fully characterized.

From equation (7) we can directly understand under what conditions HHG does or does not follow the conventional scenario of classical emission (that is, of harmonics in a multi-mode coherent state). Specifically, if the atoms are in a state with a well-defined large-N classical limit, then $\hat{\mathbf{S}}\approx\langle\hat{\mathbf{S}}\rangle$ and every mode $\hat{a}_n$ is approximately a coherent state of parameter $\alpha_n+(\mathbf{u}_n+\mathrm{i}\mathbf{v}_n)\cdot\langle\hat{\mathbf{S}}\rangle$. More precisely, when the atoms are all in the same single-particle state $|\mathbf{s}\rangle$ with $\hat{\boldsymbol{\sigma}}_j|\mathbf{s}\rangle_j=\mathbf{s}\,|\mathbf{s}\rangle_j$, then $\hat{\mathbf{S}}=N\mathbf{s}$ and the combined output state of multiple harmonics is a multi-mode coherent state $|\psi_{\mathrm{harmonics}}\rangle\approx\prod_n|\alpha_n+N(\mathbf{u}_n+\mathrm{i}\mathbf{v}_n)\cdot\mathbf{s}\rangle$. This is the case for conventional (ground state) HHG, which has $\mathbf{s}=-\mathbf{e}_z$. We note in passing that these considerations allow to maximize the yield of the nth harmonic by just finding the orientation $\mathbf{s}$ that maximizes $|\alpha_n+N(\mathbf{u}_n+\mathrm{i}\mathbf{v}_n)\cdot\mathbf{s}|$, and by preparing the atoms to such orientation with a simple coherent (rotation) pulse before the strong drive.

However, if the system is in a quantum correlated many-body state lacking a clear classical limit, the replacement $\hat{\mathbf{S}} \to \langle \hat{\mathbf{S}} \rangle$ in equation (7) becomes illegitimate, and $\hat{\mathbf{S}}$ should be considered with its full-fledged operatorial nature. This is the most interesting scenario, in which the emitted light can strongly deviate from a multi-mode coherent state.

Moreover, from a computational point of view, equation (7) provides a way to represent the harmonics' photon operators $\hat{a}_n$ as sparse $(N+1)\times(N+1)$-dimensional matrices. Indeed, the collective spin operators $\hat{\mathbf{S}} = (\hat{S}_x, \hat{S}_y, \hat{S}_z)$ have a standard and well-known matrix representation, and the whole complexity of the theory lies now in the terms α_n, $\mathbf{u}_n$ and $\mathbf{v}_n$, which can be found by solving the HHG dynamics in equation (4) (accounting for the full atomic spectrum including its continuum) and that can be conveniently computed once and for all, in the sense that they do not change when changing the number of atoms nor their initial condition. Instead, the terms α_n, $\mathbf{u}_n$ and $\mathbf{v}_n$ depend on the specific structure of the atoms and on the drive. As a limit case, we note that $|\alpha_n|$, $|\mathbf{u}_n|$ and $|\mathbf{v}_n|$ vanish for vanishing drive intensity, in which case the created photonic states $\hat{a}_n$ in equation (7) are simply the vacuum state (no emission).

The theory above allows in particular to compute normally ordered moments $\left\langle \left(\hat{a}_n^\dagger\right)^m (\hat{a}_n)^l \right\rangle = \mathrm{Tr}\left(\hat{\rho}(0)\left(\hat{a}_n^\dagger\right)^m (\hat{a}_n)^l\right)$, for which the vacuum term $\hat{a}_n(0)$ in equation (7) can be omitted. Containing the full information on the emission, these moments can be used to reconstruct, for each harmonic and for a given atomic initial condition $\hat{\rho}(0)$, the Wigner function $W(\alpha)$, the photon statistics, the normalized second-order correlation function $g^{(2)}(0) = \left\langle \hat{a}_n^\dagger \hat{a}_n^\dagger \hat{a}_n \hat{a}_n \right\rangle / \left\langle \hat{a}_n^\dagger \hat{a}_n \right\rangle^2$ and the Mandel Q parameter $Q = \left\langle \hat{a}_n^\dagger \hat{a}_n \right\rangle (g^{(2)}(0) - 1)$ (Supplementary Sect. S5). Indeed, our theory provides access to much more than that, namely it allows to compute any multi-mode normally ordered moment $\left(\hat{a}_{n_1}^\dagger\right)^{m_1}\left(\hat{a}_{n_2}^\dagger\right)^{m_2} \ldots (\hat{a}_{n_1})^{l_1}(\hat{a}_{n_2})^{l_2} \ldots$, from which the full information on the joint multi-mode state of the harmonics $n_1, n_2, \ldots$, including on the entanglement among them, can in principle be reconstructed. As an example, we use the two-mode moments to compute the joint photon number statistics of two modes and the associated Parson correlation coefficient and mutual information. Finally, to help visualize the atomic state at times $t \le 0$, we also compute the Wigner function of the atomic system on the Bloch sphere (whose axes can be thought of as corresponding to $\hat{S}_x$, $\hat{S}_y$ and $\hat{S}_z$)[39].

As for $\hat{H}^i_{\mathrm{atom}}$ in equation (1), in the following we follow convention in strong field physics and model each emitter as a single electron in a one-dimensional trapping potential[22,37,38,40]. Specifically, we consider a single-particle Hamiltonian $\hat{H}^i_{\mathrm{atom}} = \frac{\hat{p}_i^2}{2} + V(\hat{x}_i)$, with $\hat{x}_i$ and $\hat{p}_i$ the conjugate position and momentum operators of the ith atom, respectively, $V(x) = -\frac{1}{\sqrt{x^2+a^2}} + V_{ab}$ a softened Coulomb potential and V_{ab} an imaginary potential accounting for absorbing boundaries to avoid unphysical reflections of the electrons[41]. The parameter a is set to 0.816 to match the ionization potential of Ne, $I_p = 0.792$ (ref. [41]).

We finally note that, alternatively, equation (7) can be solved efficiently within a phase space approximation upon replacing the atomic operators $\hat{\mathbf{S}}$ with an ensemble of classical initial conditions on the Bloch sphere that reflects the quantum fluctuations of the actual initial wavefunction (see Supplementary Sect. S8 for details).

Emitted radiation from strongly driven many-body systems

We now use our formalism to numerically investigate the properties of the radiation emitted from a many-body atomic system. We will discuss quantum features of HHG that deviate from the established expectation (that the emitted light is coherent[14,26,36]) in a way that depends on the correlations among the atoms. We consider a strong monochromatic coherent drive $E_c(t)$ at a frequency ω_d and with a trapezoidal pulse shape (with the amplitude increasing linearly to its maximum E_0 during the first quarter of the pulse and decreasing to 0 during the last). The spectrum of the resulting emitted radiation is depicted in Fig. 1b and features the distinctive traits of HHG, namely a comb of peaks at the odd harmonics extending over a plateau up to a cut-off frequency[21,22].

Beyond reproducing these well-known features of HHG, which also emerge from a classical single-atom theory[21,22], our method also captures genuinely quantum many-body ones. For instance, Fig. 2 shows the photon number statistics and Wigner function for selected harmonics and atomic initial conditions. For conventional HHG, for which all the atoms are initially in their ground state $|\Downarrow\rangle \equiv \otimes_{i=1}^N |g\rangle_i$ (Fig. 2, left column), we confirm expectations showing an essentially coherent emission: at the odd harmonics, the correlation function $g^{(2)}$, the Wigner function and the photon statistics are almost perfectly unitary, Gaussian and Poissonian, respectively. In fact, the classical character of the emission persists as long as the atoms are initially in an uncorrelated product state, for example, $|\Rightarrow\rangle \equiv \otimes_{i=1}^N \frac{|g\rangle_i + |e\rangle_i}{\sqrt{2}}$, which can be easily obtained from $|\Downarrow\rangle$ with a coherent $\pi/2$ pulse (Fig. 2, central column). These results can be understood from equation (7) upon replacing $\hat{\mathbf{S}}$ with its classical limit, namely $-N\mathbf{e}_z$ for $|\Downarrow\rangle$ and $N\mathbf{e}_x$ for $|\Rightarrow\rangle$. The emission is in this case classical, consisting of a cross product of coherent states $|\psi_{\mathrm{harmonics}}\rangle \approx \prod_n |\alpha_n - N(\mathbf{u}_{n,3} + \mathrm{i}\mathbf{v}_{n,3})\rangle$ and $|\psi_{\mathrm{harmonics}}\rangle \approx \prod_n |\alpha_n + N(\mathbf{u}_{n,1} + \mathrm{i}\mathbf{v}_{n,1})\rangle$, respectively. In this case of emission from uncorrelated atoms, any deviation of the output light from a coherent state is due to the error in the replacement $\hat{\mathbf{S}} \to \langle \hat{\mathbf{S}} \rangle$, which is however very small in the classical limit of large N. We can quantify the deviation from a coherent state using $g^{(2)}$, which strays from the coherent-state value 1 by $\sim 1/N$.

The situation changes drastically when many-body correlations are imprinted in the atomic state at the moment of interaction with the drive field ($t = 0$), for which the atomic state, and therefore the emission, become highly non-classical. To test this idea, in the right column of Fig. 2 we consider the system initially in the Dicke-like state $|N/2\rangle$, which is the symmetric superposition of states with half of the atoms in the ground state $|g\rangle$ and the other half in the first excited state $|e\rangle$ (in the bosonic language above, such a state is denoted $|N/2,\ N/2,\ 0,\ 0,\ 0, \ldots\rangle$). This state is strongly correlated, and its atomic Wigner function on the Bloch sphere appears as a ring with weak fringes embracing the equator. For comparison, such a Wigner function is fundamentally different from that of the uncorrelated states $|\Downarrow\rangle$ and $|\Rightarrow\rangle$, which appear as two blobs around the south and east poles, respectively. The difference in the atomic state gets mirrored onto the emission: while the radiation from $|\Downarrow\rangle$ and $|\Rightarrow\rangle$ is classical, in the sense of close to coherent, that from $|N/2\rangle$ is very much not so, its photon statistics and Wigner functions being strongly non-Poissonian and non-Gaussian, respectively.

The difference in photon statistics can be quantified by the normalized second-order correlation function $g^{(2)}$, that, for instance, for the 21st harmonics takes values of 1.00002 and 1.71 for initial atomic states $|\Downarrow\rangle$ and $|N/2\rangle$, respectively. Indeed, in the latter case, the correlations initially imprinted in the atoms can result in more strikingly quantum features, such as ring-shaped Wigner functions and double-peaked photon distributions, which appear to interpolate between a thermal and a coherent state.

Intuition into the shape of the photonic Wigner function is provided by equation (7). Therein, the term $(\mathbf{u}_n + \mathrm{i}\mathbf{v}_n)\cdot\hat{\mathbf{S}}$ acts as a projection from the three-dimensional space of the atomic Bloch sphere onto the plane individuated by $\mathbf{u}_n$ and $\mathbf{v}_n$, which becomes the plane of the two quadratures of a_n. The constant α_n corresponds to a coherent shift, and the term $\hat{a}_n(0)$ adds vacuum fluctuations with a blurring effect. In this sense, the non-trivial atomic state on the Bloch sphere gets mirrored onto a non-trivial output photonic state.

https://doi.org/10.1038/s41567-022-01910-7

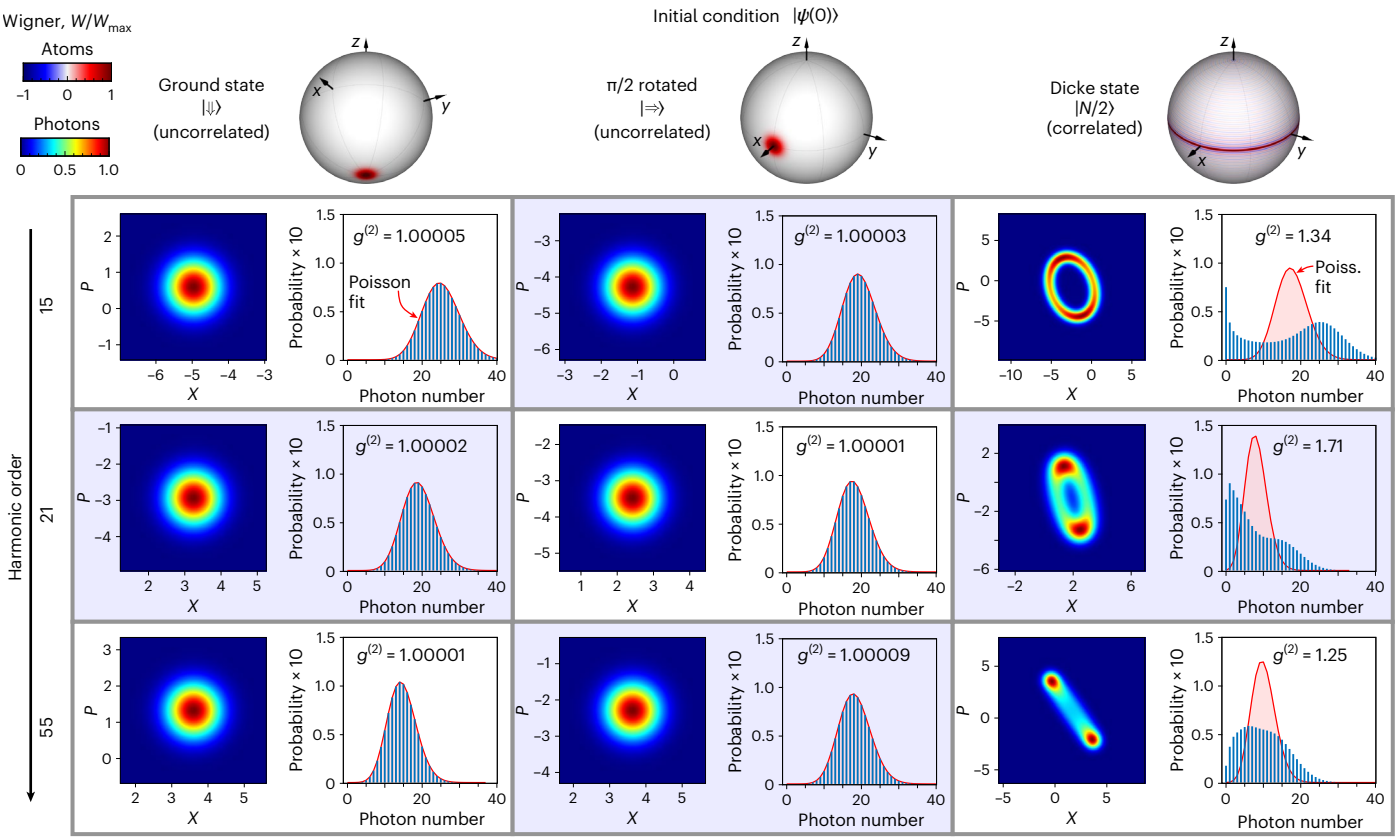

Fig. 2 | Many-body HHG. We investigate the emission for some representative odd harmonics ($n = 15$, 21 and 55 in the top, middle and bottom rows, respectively) and from selected atomic initial conditions ($|\Downarrow\rangle$, $|\Rightarrow\rangle$ and $|N/2\rangle$ in the left, centre and right columns, respectively). To help visualize the atomic initial conditions, we plot their Wigner function on the Bloch sphere (normalized with respect to their maximum value W_{max}). The HHG emission from atoms initially in the ground state $|\Downarrow\rangle$ is essentially coherent and, thus, classical (left column). The Wigner function of the input atomic state is Gaussian (around the south pole on the Bloch sphere), like the Wigner function of the output HHG emission, plotted in the plane of the two quadratures X and P. The photon number statistics is excellently fitted by a Poisson distribution (red), and the normalized second-order correlation function $g^{(2)}$ (blue) is close to 1 (deviations are of order $1/N$). The classical character of the emission holds for other uncorrelated initial conditions, such as the state $|\Rightarrow\rangle$, obtained from $|\Downarrow\rangle$ with a π/2 coherent pulse (central column). In striking contrast, strong correlations in the initial condition, for example, for the state $|N/2\rangle$, whose atomic Wigner function embraces the Bloch sphere like a belt around the equator, result in highly non-classical light (right column). Indeed, the Wigner distribution and photon statistics at the odd harmonics are strongly non-Gaussian and super-Poissonian, respectively. For instance, in the case of the 15th harmonic, we observe doubly peaked photon statistics. The simulations in these panels assume $\hbar\omega_d = 1.55$ eV, $E_0 = 60$ GV m^{-1}, $N = 6.2 \times 10^4$ and 40 cycles of the drive. The atomic Wigner functions were obtained for $N = 100$.

Engineering and controlling states of light

In the previous section, simulating emission from the state $|N/2\rangle$ helped emphasize the role of atomic correlations in creating unusual states of light, showing the concept of non-classical light emission from non-classical states of the emitters[42,43]. However, the Dicke-like state $|N/2\rangle$ might be challenging to realize in experiments, and thus we propose two different schemes that use coherent control[44] (starting from atoms initially in their ground state) to induce atomic correlations that resemble the ones of the $|N/2\rangle$ state, resulting in non-classical light emission akin to that from $|N/2\rangle$ (Figs. 3 and 4). In each scheme, we find the same concept: that the strongly driven many-body systems can generate bright and strongly non-coherent radiation. The schemes that we propose consist of three main steps: (1) a short preparation pulse brings the atoms into a coherent superposition of excited and ground states, (2) correlations between atoms build up under the system's own dynamics throughout a hold time t_h and (3) the main driving pulse is applied, resulting in HHG emission with unconventional properties. For concreteness, we will consider the scenario in which correlations result from inter-atomic interactions, and one in which they are induced through super-radiance (for details and complementary results, see Supplementary Sects. S3 and S7).

Let us begin by considering the scenario in which atomic correlations are induced through super-radiance[31,32] (Fig. 3). Super-radiance is the phenomenon whereby the spontaneous emission from an ensemble of excited emitters can be much stronger than one would expect if they emitted independently. With a long history, super-radiance has played an important role in optics and quantum mechanics, for instance with applications in quantum metrology[45], as well as in relativity and astrophysics[46]. Crucially, super-radiance creates quantum correlations among the atoms, induced by their joint interaction with the surrounding electromagnetic field. Here, we exploit this feature of super-radiance to controllably prepare the atoms in a correlated state, resulting in non-classical HHG upon subjecting the system to a strong drive. The specific protocol we consider is illustrated in Fig. 3a, and unfolds as follows: A coherent π pulse brings the atoms from $|\Downarrow\rangle$ to $|\Uparrow\rangle \equiv \otimes_{i=1}^{N} |e\rangle_i$ at time $t = -t_h$. From $|\Uparrow\rangle$, the system tends to decay back to $|\Downarrow\rangle$ via super-radiance, which involves the build up of correlations between atoms. The super-radiance process is however intermitted by the beginning of the HHG pulse after a time t_h, that is, at time $t = 0$. The parameter t_h thus offers a handle to control the initial atomic condition $\hat{\rho}(0)$ of the HHG emission. More explicitly, we find $\hat{\rho}(0)$ by numerically

https://doi.org/10.1038/s41567-022-01910-7

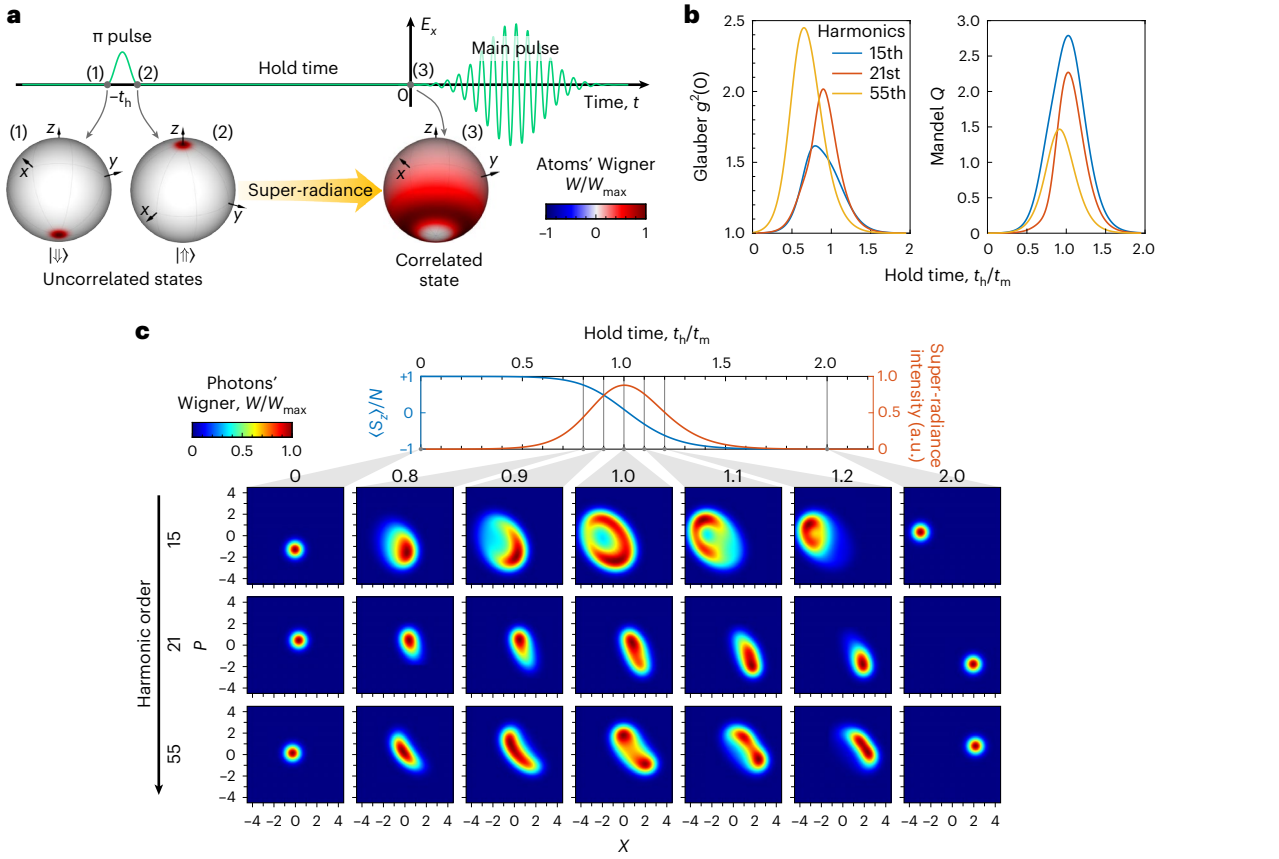

Fig. 3 | Quantum light from strongly driven super-radiant atoms. Super-radiance is exploited as a means to induce correlations in the atomic initial condition $\hat{\rho}(0)$, leading to unconventional HHG. **a**, Schematic representation of the adopted three-step protocol in which the atoms (1) are excited from $|\Downarrow\rangle$ to $|\Uparrow\rangle$ with a π pulse, (2) decay through super-radiance over a hold time t_h and (3) are subjected to a strong drive pulse leading to HHG. **b**, The correlation function $g^{(2)}(0)$ and Mandel Q parameter of the emitted harmonics depend on the amount of atomic correlations at $t = 0$, that is, on the hold time t_h. **c**, The Wigner functions of the harmonics are approximately Gaussian for $t_h = 0$ (for which $\hat{\rho}(0) = |\Uparrow\rangle\langle\Uparrow|$) and $t_h \gg t_m$ (for which $\hat{\rho}(0) \approx |\Downarrow\rangle\langle\Downarrow|$), whereas they develop non-coherent features for intermediate hold times t_h in the order of t_m. In particular, for $t_h = t_m$ the emission is highly non-classical and looks reminiscent of that from the Dicke state $|N/2\rangle$. On top, the time profiles of atomic magnetization and emission intensity are reported. The vertical gray lines serve as a reference and correspond to the hold times for which the Wigner function of the output harmonics is shown. These simulations considered $\omega_d = 1.55$ eV, $E_0 = 60$ GV m^{-1}, $\gamma N = 0.1$, $N = 3.7 \times 10^4$ and 40 cycles of the drive. The atomic Wigner functions on the Bloch spheres in **a** were obtained for $N = 100$ and $t_h = 1.3t_m$.

integrating from $t = -t_h$ to $t = 0$ the following collective Lindblad master equation describing super-radiance[32,47,48]:

$$\frac{d\hat{\rho}}{dt} = \gamma\left(\hat{S}^-\hat{\rho}\hat{S}^+ - \frac{1}{2}\left\{\hat{S}^+\hat{S}^-, \hat{\rho}\right\}\right), \tag{8}$$

With γ the emission rate and starting from $\hat{\rho}(-t_h) = |\Uparrow\rangle\langle\Uparrow|$, Equation (8), whose solution is facilitated by the diagonal nature of $\hat{\rho}(t)$, captures the distinctive bell-shaped time profile of the super-radiance emission intensity, with maximum emission after a time $t_m \approx \frac{\log N}{4\gamma N}$ (ref. [32]), as well as the build-up of atomic correlations. The state of the system through the super-radiance process can be visualized in term of the atomic Wigner function on the Bloch sphere (Fig. 3a). The atomic Wigner function, initially concentrated around the north pole for $\hat{\rho}(-t_h) = |\Uparrow\rangle\langle\Uparrow|$, 'cascades' around the Bloch sphere during super-radiance. Halfway through the decay, the atomic Wigner wraps the sphere in a way that is reminiscent of the Wigner function of the Dicke state $|N/2\rangle$ in Fig. 2, although with a much wider broadening along the z axis. This perspective suggests that we should be able to obtain non-classical emission akin to that from $|N/2\rangle$.

The second-order correlation function $g^{(2)}(0)$ and Mandel Q parameter of the emission resulting from a strong drive are shown in Fig. 3b for a few selected harmonics. A classical emission ($g^{(2)}(0) = 1$ and $Q = 0$) is obtained for both $t_h = 0$, for which super-radiance does not have the time to start and $\hat{\rho}(0) = |\Uparrow\rangle\langle\Uparrow|$, and for $t_h \gg t_m$, for which super-radiance makes all atoms decay and $\hat{\rho}(0) \approx |\Uparrow\rangle\langle\Uparrow|$. In between these two limit cases, $\hat{\rho}(0)$ is non-trivial and accounts for correlations among the atoms, which directly translates onto a non-classical emission with harmonics strongly deviating from a coherent state ($g^{(2)}(0) > 1$ and $Q > 0$). The full portrait of the harmonics is given in Fig. 3c in terms of photonic Wigner functions. These are approximately Gaussian for $t_h = 0$ and $t_h \gg t_m$ but acquire a richer structure for intermediate t_h. In particular, for $t_h = t_m$, that is, shining the strong drive pulse onto the system when its super-radiance intensity is at its maximum, we find, as hoped, photonic Wigner functions reminiscent of those obtained for $|N/2\rangle$ in Fig. 2, although more blurred.

Second, we exemplify the concept of HHG from a many-body system correlated through interactions by considering the case in which, before the pulse (that is, at $t < 0$), the atomic system is described by the one-axis twisting Hamiltonian[33]

$$\hat{H} = \frac{\omega_0}{2}\hat{S}_z + \frac{\omega_J}{N}\hat{S}_z^2. \tag{9}$$

In equation (9), the first term is nothing but the original $\hat{H}^i_{atom}$ but restricted to the two lowest single-particle levels $|g\rangle$ and $|e\rangle$, with

https://doi.org/10.1038/s41567-022-01910-7

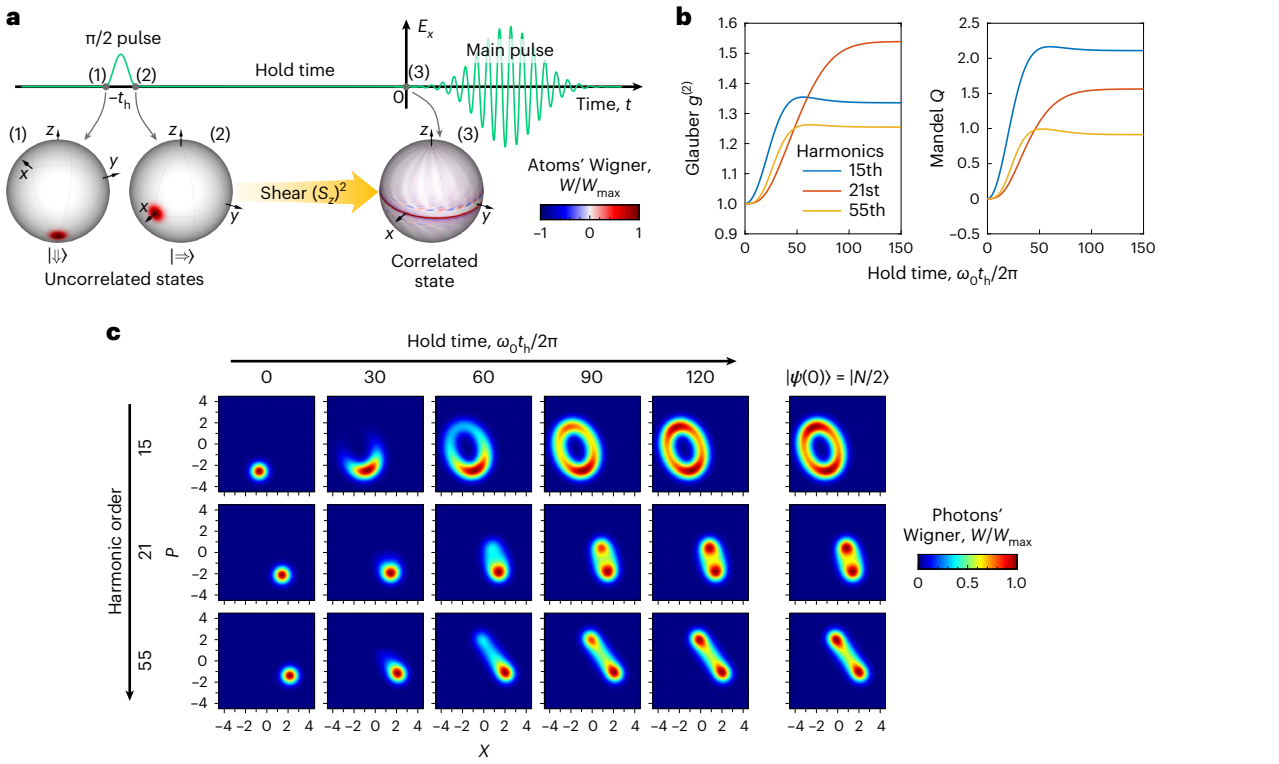

Fig. 4 | Quantum light from strongly driven interacting atoms. The physics and structure of this figure are in analogy to Fig. 3, but exploiting inter-atomic interactions, rather than super-radiance, to induce the atomic correlations underpinning non-classical HHG. **a**, Specifically, we consider that: (1) a preparation π/2 pulse is applied to atoms initially in their ground state, (2) atomic correlations build up via inter-atomic interactions throughout a hold time t_h and (3) the system is illuminated with an intense drive laser pulse, resulting in HHG. **b**, The correlation function $g^{(2)}(0)$ and Mandel Q parameter of the emitted light depend on the amount of correlations in the atomic system at the time of the strong pulse, that is, on the hold time t_h, with $t_h = 0$ the limit of classical coherent emission from uncorrelated atoms. **c**, The properties of the emission are more comprehensively illustrated by the Wigner distributions of the harmonics of interest. Starting from Gaussian for $t_h = 0$, these are deformed for $t_h > 0$, becoming for $t_h\omega_0/2\pi \gtrsim 120$ very close to those obtained for atoms initially in $|N/2\rangle$ (reported in the right column as a reference). Here, we considered $\omega_d = 1.55$ eV, $E_0 = 60$ GV m^{-1}, $\omega_J = 2.7$ eV, $N = 37{,}000$ and 40 cycles of the drive. The atomic Wigner functions on the Bloch spheres in **a** were obtained for $N = 100$ and $\omega_J t_h = 50$.

$\omega_0 = 0.49$ the energy difference between them. The second term, of strength ω_J and normalized by N to guarantee extensivity, accounts instead for a collective interaction. This can, for instance, occur in trapped cold atoms in optical cavities[49,50] and is standard in the context of spin squeezing[33]. But most importantly, from a theoretical perspective, the Hamiltonian in equation (9) preserves the atoms' permutational symmetry, allowing the theoretical framework above to be readily applied.

The protocol we consider, illustrated in Fig. 4a, closely follows that introduced by Kitagawa and Ueda in their seminal work for spin squeezing[33]: a π/2 pulse brings the atoms in the state $|\Rightarrow\rangle$, from which correlations develop under the action of the twisting term $\hat{S}_z^2$ in equation (9). The action of the latter can be effectively visualized in terms of the atomic Wigner function on the Bloch sphere, which gets progressively more and more sheared, wrapping around the Bloch sphere to embrace its equator. This perspective suggests how, for long enough hold times t_h, the state of the atoms becomes akin to that of $|N/2\rangle$, whose Wigner function was indeed a ring encircling the equator (Fig. 2). By tuning the hold time t_h separating the two pulses, we can therefore interpolate from a regime of classical emission from an uncorrelated atomic state $|\Rightarrow\rangle$ to one of strongly non-classical emission form a strongly correlated atomic state akin to $|N/2\rangle$. In Fig. 4b, this is shown in terms of the second-order correlation function $g^{(2)}(0)$ and Mandel Q parameter, taking for $t_h = 0$ values of 1 and 0, respectively and corresponding to coherent emission, and larger values for $t_h > 0$. Figure 4c instead shows the Wigner function of the emitted light, showing how, starting from Gaussian for $t_h = 0$, it gets deformed for $t_h > 0$, becoming for long enough t_h completely analogous to that resulting from atoms initially in $|N/2\rangle$, which we report as a reference.

We finally investigate the correlations between different harmonics. The qualitative finding is that, while the harmonics are in a separable state in conventional ground-state HHG, they become correlated when the atoms are prepared in a correlated state. To facilitate this finding, we focus for concreteness on the second scheme considered above, that of interaction-induced correlations, and compute the joint photon statistics between two harmonics n and m, that is, the probability $p(k_n, k_m)$ to observe k_n photons in the mode n and k_m photons in the mode m (Fig. 5a). By changing t_h, we can again interpolate between an uncorrelated atomic state for $t_h = 0$ and a correlated atomic state akin to $|N/2\rangle$ for large t_h. To quantify the degree of interdependence between the two harmonics, from the joint photon number statistics $p(k_n, k_m)$, we compute the Parson correlation coefficient $c = \frac{\mathrm{cov}(k_n, k_m)}{\sigma_{k_n}\sigma_{k_m}}$, with $\mathrm{cov}(k_n, k_m)$ the covariance of the photon numbers and σ_{k_n} and σ_{k_m} their s.d., and the mutual information $I_{mn} = \sum_{k_n,k_m} p(k_n, k_m) \log \frac{p(k_n,k_m)}{p(k_n)p(k_m)}$. Figure 5b shows these diagnostics to vanish for $t_h = 0$, meaning that the harmonics are uncorrelated if the atoms are. By contrast, initially correlated atoms ($t_h > 0$) result in statistically dependent ($I_{mn} > 0$) harmonics. The correlation between two harmonics can be both positive ($c > 0$, as for the 21st and 55th harmonics) or negative ($c < 0$, as for the 15th and 21st harmonics).

https://doi.org/10.1038/s41567-022-01910-7

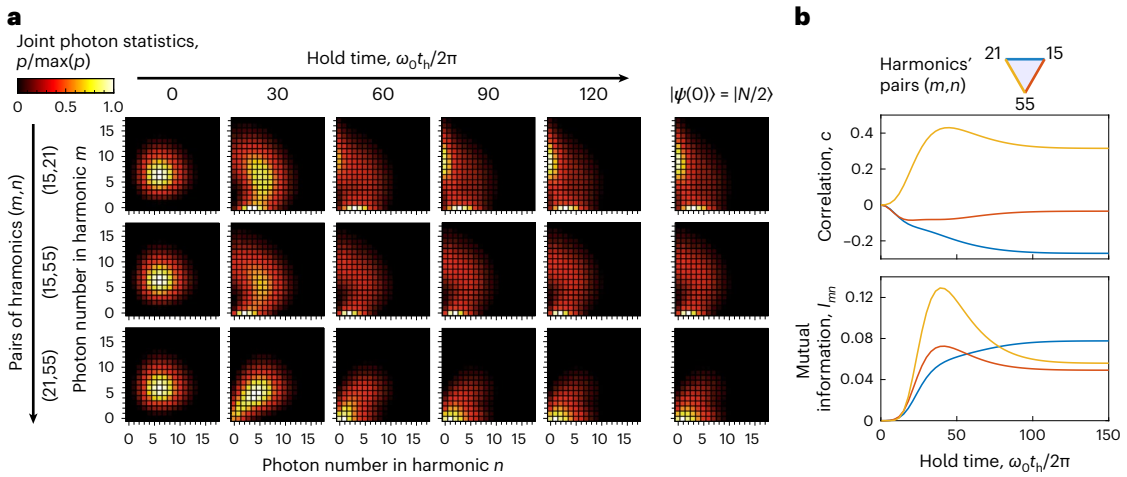

Fig. 5 | Correlated states of light. Using the same protocol as in Fig. 4, we show that preparing the atoms in a correlated state results in strong correlations between different output harmonics. **a**, The joint photon statistics for selected pairs of harmonics (one pair per row) becomes increasingly non-trivial for larger hold times t_h (one time per column), that is, for stronger initial atomic correlations. For $t_h\omega_0/2\pi \gtrsim 120$, the joint photon statistics becomes very close to that obtained from the state $|N/2\rangle$, reported in the last column as a reference. **b**, The Parson correlation coefficient c and the mutual information I_{mn} are witnesses of the entanglement between harmonics pairs, vanish for $t_h = 0$ (that is, uncorrelated atomic initial condition) and are finite otherwise. The considered pairs of harmonics are 21-15 (blue), 15-55 (red), and 55-21 (yellow). Here, we used the same parameters as in Fig. 4.

Path towards experimental realization. Many of the quantum-optical properties we predict for HHG should be within the reach of state-of-the-art experiments. The photon statistics, Glauber correlation coefficient $g^{(2)}$ and Mandel parameter Q of the harmonics of interest can all be computed from photon counting measurements averaged over repeated experiments. Such measures should clearly distinguish emission by atoms imprinted with strong correlations relative to emission of classical light (for example, $g^{(2)} > 2$ in Fig. 3 versus $g^{(2)} = 1$ for a coherent state). Indeed, for uncorrelated atoms in conventional HHG, the deviation of the emitted harmonics from a (classical) perfectly coherent multi-mode state are small, as shown in Fig. 2 and refs. [14,26]. The joint photon statistics, correlation coefficient and mutual information between two harmonics (Fig. 5) could also be extracted by photon counting detectors. Finally, the Wigner function of the emitted harmonics could be reconstructed via homodyne detection[51–53]. The lower harmonics could be characterized in this way by established conventional means for homodyne detection in the visible range. Homodyne schemes for the higher harmonics (UV, XUV or soft-X-ray frequencies) will require new developments, which are gradually becoming feasible (for example, interferometers and sub-cycle delay lines in the XUV[54–56]).

In our one-dimensional atomic model, we set $a = 0.816$ to best mimic the spectrum of Ne. The choice of potential can be readily revised to model other emitting systems. In fact, more realistic simulations can be obtained by considering three-dimensional atomic Hamiltonians for $\hat{H}^i_{\mathrm{atom}}$, or directly replacing the particle energies W and dipole moments D in equation (4) by values extracted from a density functional theory simulation. This choice does not change the structure of the theory itself, and thus the conclusions are independent of the details of the model. The form and interpretation of equation (7) remain unchanged (only the values of α_n, $\mathbf{u}_n$ and $\mathbf{v}_n$ would change), meaning that the qualitative results we found carry over to more realistic scenarios. Indeed, this establishes the generality of the concept that we put forward, that of non-classical emission from correlated strongly driven many-body systems.

A core assumption in our theoretical derivation is that of indistinguishable atoms. This Dicke-like assumption makes the notoriously hard many-body problem tractable. The main findings of the theory are conveyed by equation (7), which shows the transfer of the non-classical states of the input emitters to the non-classical states of the output light. The assumption of indistinguishable atoms is legitimate, for instance, when large collections of atoms occupy a small volume as compared with the involved radiation wavelengths. To have a concrete estimate of the number of atoms N fulfilling this criterion, consider a drive wavelength of $\lambda = 800$ nm creating the $n = 15$th harmonic, with wavelength $\lambda_n = \lambda/n = 53$ nm. The volume in which atoms can be considered indistinguishable is $V \approx (\lambda_n/2)^3$. For an ideal gas, the number of particles within such a volume reads $N = \frac{pV}{RT}N_A$, with p, R, T and N_A the pressure, gas constant, temperature and Avogadro number, respectively. At room temperature and atmospheric pressure, we get $N \approx 500$, and larger N values similar or beyond those simulated in in Figs. 3–5 could be obtained for example just by increasing the pressure and/or lowering the temperature[57]. The number N can be even greater within the emerging field of solid-state HHG, which is now widely explored experimentally (see, for example, refs. [58–60]). Given that the atomic spacing between atoms in solids is usually of a few angstroms, one finds $N \approx 10^5$ to 10^6 for the same volume above. Interestingly, it might be possible to arrange the atoms over a larger volume (extending over many wavelengths) such that they can be effectively considered indistinguishable, for example, thanks to phase matching in atomic ensembles[47,48].

In any case, the general concept of non-classical emission in HHG from non-classical many-body states of emitters is likely much broader than the indistinguishability assumption that we used here to show it. Indeed, numerous many-body phenomena have traditionally been first studied within a similar assumption, before being extended far beyond it. This idea applies to countless phenomena in and out of equilibrium, including those leveraged by the preparation schemes adopted in Figs. 3–5 here, namely super-radiance[31,32] and spin squeezing[33]. We expect the theory of strongly driven many-body systems to follow a similar path.

The approximation of indistinguishable atoms has here also been adopted to model the preparation stages, in which correlations in the atomic ensemble are induced via either super-radiance or inter-atomic interactions. In the case of super-radiance, the indistinguishability assumption is, for example, justified when the atoms are within a volume $V \approx (\lambda_0/2)^3$ (ref. [32]), where $\lambda_0 = 92$ nm is the wavelength associated to the transition $|e\rangle \rightarrow |g\rangle$ and that is anyway a less stringent condition

than that analysed above with the wavelength λ_n of the harmonic $n = 15$, given that $\lambda_0 > \lambda_n$. In the case of interaction-induced correlations, relevant systems include strongly interacting gases of atoms or molecules, whose interactions can be enhanced by trapping them in optical cavities. Such systems can realize the infinite-range (all-to-all) $\hat{S}_z^2$ interactions (shear force terms) discussed in the previous section[49,61]. Moreover, finite-range spin–spin interactions, which are ubiquitous in many hot vapour[62] and cold atom systems[63], can also realize spin-squeezed states[64,65] and thus should also show variants of the quantum features we proposed here. Another promising platform for exploring these ideas is Rydberg atoms[49,50,66], offering the possibility of controllably generating correlated many-body atomic states[67,68].

Note that the collective forms of the super-radiant decay and interactions in equation (8) and (9), respectively, have been chosen for pure tractability reasons, and do not represent a limitation to the validity of our general concept of emission by strongly driven correlated many-body systems. In fact, any procedure that creates non-classical states of atoms can result, in light of equation (7), in non-classical output harmonics.

Finally, Dicke states such as $|N/2\rangle$ could in principle be prepared via post-selection in super-radiance. Specifically, if one could measure the number n_{super} of photons spontaneously emitted during super-radiance (as described by equation (8)), the atoms would then collapse in the state $|N - n_{\mathrm{super}}\rangle$ consisting of a symmetric superposition of n_{super} atoms in the ground state $|g\rangle$ and $N - n_{\mathrm{super}}$ atoms in the first excited state $|e\rangle$. For $n_{\mathrm{super}} \approx N/2$, this initial condition would lead to emission similar to that obtained for $|N/2\rangle$ in Fig. 2.

Discussion and outlook

Our work proposes strongly driven many-body systems to realize many-photon states of light with controllable quantum features and over a broad spectral range up to X-ray frequencies. At the core of this concept is the idea that non-classical states of the emitters get reflected onto non-classical states of the emission. For example, equation (7) shows how the Wigner function of the atoms (on the Bloch sphere) gets effectively projected onto that of the emitted harmonics (in the plane of the two quadratures of light) (for example, Fig. 2). The paradigm of classical coherent emission in HHG, well established for conventional HHG from atoms initially in their single-particle ground states, can now be overcome: if the atoms are strongly correlated, the output harmonics exhibit strongly non-coherent features, such as doubly peaked photon statistics and intra-harmonic correlations. The challenge of engineering strongly non-classical states of light is therefore shifted to the comparably simpler one of preparing strongly correlated atomic states. We considered but two examples, in which the atomic correlations are dynamically generated under the system's own (undriven) dynamics during a preparation stage, via either super-radiance or inter-atomic interactions acting throughout a hold time t_{h} between an excitation and the HHG pulses. Varying t_{h}, one can control the amount of correlations in the atoms and therefore the deviation of the harmonics from a multi-mode coherent state.

The ideas presented here have several potential applications. We showed that HHG emission from a correlated system has super-Poissonian statistics and a broadband spectrum (for example, $g^{(2)} > 2.0$ in Fig. 3). Such bunched light could be used to enhance the efficiency of certain non-linear processes driven by the high harmonics. For comparison, in the optical range, it has been shown that, for bright squeezed vacuum light (for which $g^{(2)} = 3$), the efficiencies of the $\chi^{(2)}$ and $\chi^{(3)}$ non-linearities increase by a factor ~3 and ~14, respectively[10]. The increased efficiencies motivate using our bunched high harmonics to drive processes that relate to $\chi^{(2)}$ and $\chi^{(3)}$, such as second- and third-harmonic generation, which could lead to even higher frequencies, producing super-Poissonian X-ray light.

The correlations between different harmonics offer new prospects for enhancing the signal-to-noise ratio in quantum imaging[69]. Such correlations have not been predicted by previous theories of HHG. The correlations between widely different harmonics could be particularly relevant for biological samples, which are very sensitive to ionizing radiation and specifically X-ray light in the water transparency window that can be reached using HHG[70]. For instance, we envision using the correlations between harmonics to acquire an image by measuring photons of a different frequency than the one interacting with the target sample.

Finally, our work suggests HHG as a probe to characterize many-body states of matter. For instance, by measuring the Wigner function of the output harmonics[51–53], it should be possible via equation (7) to reconstruct the atomic Wigner function, thus accessing information on the many-body state of the atoms with high temporal resolution[19,20]. One of the most interesting implementations of our general concept would be to try to image the attosecond dynamics of vortices in superfluids and superconductors[71], Bose–Einstein condensates[72] and other strongly correlated many-body systems. The quantum correlations in such phenomena could be transferred to the quantum state of light and thus inferred by quantum-optical means.

The theory that we developed can be adopted or generalized in several different research directions. One question worth pursuing regards further ways of controlling the atomic initial conditions and thus the emitted radiation, for instance, involving more than just the two lowest single-particle levels. Beyond HHG, our theory can then be readily generalized to any strongly driven many-body system that emits radiation: further work should investigate the possibility of engineering not only the initial condition of the atoms but also the temporal profile of the driving pulse. An ambitious generalization of the theory could investigate the effects of the spatial distribution of the atoms, for example, in solids, going beyond the approximation of indistinguishable atoms. Looking forward, our work contributes to the ambitious goal of bringing together quantum optics and attoscience, suggesting a new path towards the realization of fully tuneable sources of intense quantum light in new spectral ranges.

Online content

Any methods, additional references, Nature Portfolio reporting summaries, source data, extended data, supplementary information, acknowledgements, peer review information; details of author contributions and competing interests; and statements of data and code availability are available at https://doi.org/10.1038/s41567-022-01910-7.

References

1. Mukamel, S. et al. Roadmap on quantum light spectroscopy. *J. Phys. B* **53**, 72002 (2020).
2. Aasi, J. et al. Enhanced sensitivity of the LIGO gravitational wave detector by using squeezed states of light. *Nat. Photonics* **7**, 613–619 (2013).
3. Aasi, J. et al. Advanced LIGO. *Class. Quantum Gravity* **32**, 74001 (2015).
4. Arrazola, J. M. et al. Quantum circuits with many photons on a programmable nanophotonic chip. *Nature* **591**, 54–60 (2021).
5. Wu, L.-A., Kimble, H. J., Hall, J. L. & Wu, H. Generation of squeezed states by parametric down conversion. *Phys. Rev. Lett.* **57**, 2520 (1986).
6. Pereira, S. F., Xiao, M., Kimble, H. J. & Hall, J. L. Generation of squeezed light by intracavity frequency doubling. *Phys. Rev. A* **38**, 4931 (1988).
7. Breitenbach, G., Schiller, S. & Mlynek, J. Measurement of the quantum states of squeezed light. *Nature* **387**, 471–475 (1997).
8. Agafonov, I. N., Chekhova, M. V. & Leuchs, G. Two-color bright squeezed vacuum. *Phys. Rev. A* **82**, 11801 (2010).
9. Iskhakov, T. S., Pérez, A. M., Spasibko, K. Y., Chekhova, M. V. & Leuchs, G. Superbunched bright squeezed vacuum state. *Opt. Lett.* **37**, 1919 (2012).

10. Spasibko, K. Y. et al. Multiphoton effects enhanced due to ultrafast photon-number fluctuations. *Phys. Rev. Lett.* **119**, 223603 (2017).
11. Manceau, M., Spasibko, K. Y., Leuchs, G., Filip, R. & Chekhova, M. V. Indefinite-mean Pareto photon distribution from amplified quantum noise. *Phys. Rev. Lett.* **123**, 123606 (2019).
12. Zavatta, A., Viciani, S. & Bellini, M. Quantum-to-classical transition with single-photon-added coherent states of light. *Science* **306**, 660 (2004).
13. Ourjoumtsev, A., Tualle-Brouri, R., Laurat, J. & Grangier, P. Generating optical Schrodinger kittens for quantum information processing. *Science* **312**, 83 (2006).
14. Lewenstein, M. et al. Generation of optical Schrödinger cat states in intense laser–matter interactions. *Nat. Phys.* **17**, 1104–1108 (2021).
15. Ourjoumtsev, A., Jeong, H., Tualle-Brouri, R. & Grangier, P. Generation of optical 'Schrödinger cats' from photon number states. *Nature* **448**, 784–786 (2007).
16. Sychev, D. V. et al. Enlargement of optical Schrödinger's cat states. *Nat. Photonics* **11**, 379–382 (2017).
17. Wakui, K., Takahashi, H., Furusawa, A. & Sasaki, M. Photon subtracted squeezed states generated with periodically poled $KTiOPO_4$. *Opt. Express* **15**, 3568 (2007).
18. Deleglise, S. et al. Reconstruction of non-classical cavity field states with snapshots of their decoherence. *Nature* **455**, 510–514 (2008).
19. Paul, P.-M. et al. Observation of a train of attosecond pulses from high harmonic generation. *Science* **292**, 1689 (2001).
20. Agostini, P. & DiMauro, L. F. The physics of attosecond light pulses. *Rep. Prog. Phys.* **67**, 813 (2004).
21. Corkum, P. B. Plasma perspective on strong field multiphoton ionization. *Phys. Rev. Lett.* **71**, 1994 (1993).
22. Lewenstein, M., Balcou, P., Ivanov, M. Y., L'Huillier, A. & Corkum, P. B. Theory of high-harmonic generation by low-frequency laser fields. *Phys. Rev. A* **49**, 2117 (1994).
23. Schafer, K. J., Yang, B., DiMauro, L. F. & Kulander, K. C. Above threshold ionization beyond the high harmonic cutoff. *Phys. Rev. Lett.* **70**, 1599 (1993).
24. Tsatrafyllis, N., Kominis, I. K., Gonoskov, I. A. & Tzallas, P. High-order harmonics measured by the photon statistics of the infrared driving-field exiting the atomic medium. *Nat. Commun.* **8**, 15170 (2017).
25. Tsatrafyllis, N. et al. Quantum optical signatures in a strong laser pulse after interaction with semiconductors. *Phys. Rev. Lett.* **122**, 193602 (2019).
26. Gorlach, A., Neufeld, O., Rivera, N., Cohen, O. & Kaminer, I. The quantum-optical nature of high harmonic generation. *Nat. Commun.* **11**, 4598 (2020).
27. Mandel, L. & Wolf, E. *Optical Coherence and Quantum Optics* (Cambridge Univ. Press, 1995).
28. Scully, M. O. & Zubairy, M. S. *Quantum Optics* (Cambridge Univ. Press, 1997).
29. Gerry, C., Knight, P., & Knight, P. L. *Introductory Quantum Optics* (Cambridge Univ. Press, 2005).
30. Garrison, J. & Chiao, R. *Quantum Optics* (Oxford Univ. Press, 2008).
31. Dicke, R. H. Coherence in spontaneous radiation processes. *Phys. Rev.* **93**, 99 (1954).
32. Gross, M. & Haroche, S. Superradiance: an essay on the theory of collective spontaneous emission. *Phys. Rep.* **93**, 301 (1982).
33. Kitagawa, M. & Ueda, M. Squeezed spin states. *Phys. Rev. A* **47**, 5138 (1993).
34. Kardar, M. *Statistical Physics of Fields* (Cambridge Univ. Press, 2007).
35. Kardar, M. *Statistical Physics of Particles* (Cambridge Univ. Press, 2007).
36. Brabec, T. & Kapteyn, H. *Strong Field Laser Physics*, Vol. 1 (Springer, 2008).
37. Boyd, R. W. *Nonlinear Optics* (Academic, 2020).
38. Vrakking, M. & Schultz, T. *Attosecond and XUV Physics: Ultrafast Dynamics and Spectroscopy* (Wiley Online Library, 2014).
39. Dowling, J. P., Agarwal, G. S. & Schleich, W. P. Wigner distribution of a general angular-momentum state: applications to a collection of two-level atoms. *Phys. Rev. A* **49**, 4101 (1994).
40. Joachain, C. J., Kylstra, N. J., & Potvliege, R. M. *Atoms in Intense Laser Fields* (Cambridge Univ. Press, 2012).
41. Nurhuda, M. & Faisal, F. H. M. Numerical solution of time-dependent Schrödinger equation for multiphoton processes: a matrix iterative method. *Phys. Rev. A* **60**, 3125 (1999).
42. Gardiner, C., Zoller, P., and Zoller, P. *Quantum Noise: A Handbook of Markovian and Non-Markovian Quantum Stochastic Methods with Applications to Quantum Optics* (Springer Science & Business Media, 2004).
43. Porras, D. & Cirac, J. I. Collective generation of quantum states of light by entangled atoms. *Phys. Rev. A* **78**, 53816 (2008).
44. McCaul, G., Orthodoxou, C., Jacobs, K., Booth, G. H. & Bondar, D. I. Driven imposters: controlling expectations in many-body systems. *Phys. Rev. Lett.* **124**, 183201 (2020).
45. Paulisch, V., Perarnau-Llobet, M., González-Tudela, A. & Cirac, J. I. Quantum metrology with one-dimensional superradiant photonic states. *Phys. Rev. A* **99**, 43807 (2019).
46. Witek, H., Cardoso, V., Ishibashi, A. & Sperhake, U. Superradiant instabilities in astrophysical systems. *Phys. Rev. D.* **87**, 43513 (2013).
47. Bonifacio, R., Schwendimann, P. & Haake, F. Quantum statistical theory of superradiance. I. *Phys. Rev. A* **4**, 302 (1971).
48. Bonifacio, R., Schwendimann, P. & Haake, F. Quantum statistical theory of superradiance II. *Phys. Rev. A* **4**, 854 (1971).
49. Muniz, J. A. et al. Exploring dynamical phase transitions with cold atoms in an optical cavity. *Nature* **580**, 602–607 (2020).
50. Bernien, H. et al. Probing many-body dynamics on a 51-atom quantum simulator. *Nature* **551**, 579–584 (2017).
51. Lvovsky, A. I. & Raymer, M. G. Continuous-variable optical quantum-state tomography. *Rev. Mod. Phys.* **81**, 299 (2009).
52. Smithey, D. T., Beck, M., Raymer, M. G. & Faridani, A. Measurement of the Wigner distribution and the density matrix of a light mode using optical homodyne tomography: application to squeezed states and the vacuum. *Phys. Rev. Lett.* **70**, 1244 (1993).
53. Leonhardt, U. *Measuring the Quantum State of Light*, Vol. 22 (Cambridge Univ. Press, 1997).
54. Descamps, D. et al. Extreme ultraviolet interferometry measurements with high-order harmonics. *Opt. Lett.* **25**, 135–137 (2000).
55. Dudovich, N. et al. Measuring and controlling the birth of attosecond XUV pulses. *Nat. Phys.* **2**, 781–786 (2006).
56. Smirnova, O. et al. High harmonic interferometry of multi-electron dynamics in molecules. *Nature* **460**, 972–977 (2009).
57. Comby, A. et al. Absolute gas density profiling in high-order harmonic generation. *Opt. Express* **26**, 6001 (2018).
58. Ghimire, S. et al. Observation of high-order harmonic generation in a bulk crystal. *Nat. Phys.* **7**, 138–141 (2011).
59. Tancogne-Dejean, N., Mücke, O. D., Kärtner, F. X. & Rubio, A. Ellipticity dependence of high-harmonic generation in solids originating from coupled intraband and interband dynamics. *Nat. Commun.* **8**, 745 (2017).
60. Ghimire, S. & Reis, D. A. High-harmonic generation from solids. *Nat. Phys.* **15**, 10–16 (2019).
61. Sørensen, A. S. & Mølmer, K. Entangling atoms in bad cavities. *Phys. Rev. A* **66**, 22314 (2002).

62. Zibrov, A. S., Ye, C. Y., Rostovtsev, Y. V., Matsko, A. B. & Scully, M. O. Observation of a three-photon electromagnetically induced transparency in hot atomic vapor. *Phys. Rev. A* **65**, 43817 (2002).
63. Ritsch, H., Domokos, P., Brennecke, F. & Esslinger, T. Cold atoms in cavity-generated dynamical optical potentials. *Rev. Mod. Phys.* **85**, 553 (2013).
64. Perlin, M. A., Qu, C. & Rey, A. M. Spin squeezing with short-range spin-exchange interactions. *Phys. Rev. Lett.* **125**, 223401 (2020).
65. Ma, J., Wang, X., Sun, C.-P. & Nori, F. Quantum spin squeezing. *Phys. Rep.* **509**, 89 (2011).
66. Gallagher, T. F., *Rydberg Atoms*, Vol. 3 (Cambridge Univ. Press, 2005).
67. Omran, A. et al. Generation and manipulation of Schrödinger cat states in Rydberg atom arrays. *Science* **365**, 570 (2019).
68. Browaeys, A. & Lahaye, T. Many-body physics with individually controlled Rydberg atoms. *Nat. Phys.* **16**, 132–142 (2020).
69. Lloyd, S. Enhanced sensitivity of photodetection via quantum illumination. *Science* **321**, 1463 (2008).
70. Sayre, D., Kirz, J., Feder, R., Kim, D. M. & Spiller, E. Potential operating region for ultrasoft X-ray microscopy of biological materials. *Science* **196**, 1339 (1977).
71. Harada, K. et al. Real-time observation of vortex lattices in a superconductor by electron microscopy. *Nature* **360**, 51–53 (1992).
72. Abo-Shaeer, J. R., Raman, C., Vogels, J. M. & Ketterle, W. Observation of vortex lattices in Bose–Einstein condensates. *Science* **292**, 476 (2001).

Data availability

All the data that support the plots within this paper and other findings of this study are available from the corresponding author upon reasonable request.

Code availability

The code is available from the authors upon reasonable request.

Acknowledgements

We thank R. Bekenstein, O. Cohen, E. G. Dalla Torre, M. Even Tzur, M. Faran, R. Ruimy, E. Shahmoon and J. Sloan for insightful discussion on related topics and especially D. Malz and M. Kruger for discussions and for comments on the manuscript, and M. E. Tsur for illustrating state-of-the-art methods for simulating HHG with one-dimensional atomic models. A.P. acknowledges support from the Royal Society and from the AFOSR MURI programme (grant no. FA9550-21-1-0069), and hospitality at the Technical University of Munich (TUM).

Author contributions

All the authors made critical contributions to this work.

Competing interests

The authors declare no competing interests.

Additional information

Supplementary information The online version contains supplementary material available at https://doi.org/10.1038/s41567-022-01910-7.

Correspondence and requests for materials should be addressed to Nicholas Rivera or Ido Kaminer.

Peer review information *Nature Physics* thanks Karen Hatsagortsyan and the other, anonymous, reviewer(s) for their contribution to the peer review of this work.